

**The Emission of Relativistic Singly Charged Fragments and
the Final-State Energy Spectrum in Electromagnetic Dissociation of
 ZX into H and $Z_{i-1}Y$**

Fu-Hu Liu

*Institute of Modern Physics and Department of Physics, Shanxi Teachers University,
Linfen, Shanxi 041004, China*

(Received October 2, 2001)

We have introduced a two-source emission picture to describe the transverse momentum (P_T) distribution of relativistic singly charged fragments (H fragments) in the decay mode $ZX(^{\circ},H)Z_{i-1}Y$. The calculated results are compared and shown to be in agreement with the experimental H fragment P_T distributions in the decay mode $^{32}S(^{\circ},H)P$ and $^{16}O(^{\circ},H)N$ at 200A GeV. The final-state energy spectrum in the electromagnetic dissociation is calculated by a simple method. The final-state energy curves obtained from the calculation are in agreement with the experimental data of ^{28}Si into $p + ^{27}Al$ at an energy of 14.6A GeV.

PACS. 25.75.-q – Relativistic heavy-ion collisions.

PACS. 25.70.Mn – Projectile and target fragmentation.

I. Introduction

In high energy nucleus-nucleus collisions, three kinds of interactions were found in experiment [1]. They are elastic collisions, electromagnetic dissociations and nuclear reactions. An elastic collision is usually a very peripheral collision in an emulsion between the projectile nucleus and target hydrogen nucleus. A nuclear reaction is a violent collision between the projectile and target. An electromagnetic dissociation (EMD) is a projectile (or target) nuclear fragmentation in the virtual photon field of the target (or projectile) nucleus, or both the projectile and target fragmentations in each other's virtual photon fields. In an EMD, the impact parameter is greater than the sum of the projectile and target radii.

An EMD is caused by the electromagnetic excitation of nuclei in peripheral nucleus-nucleus collisions and can be very important at high energies, due to the relativistic enhancement of the Coulomb field of the target, as seen in the rest frame of the projectile. The fragment charge, partial cross section, transverse momentum and final-state energy of the EMD process have been measured in a number of experiments at a variety of beam energies [1-8].

The simplest EMD process is that of ZX excited by virtual photons fragments into H and $Z_{i-1}Y$, i.e., $ZX(^{\circ}, H)Z_{i-1}Y$, where Z is the atomic number of the projectile X and $^{\circ}$ denotes one or more than one virtual photons. The final state consists of a relativistic projectile singly charged fragment H and the residual nucleus Y of the projectile. In the simplest EMD process, the target does not fragment. In an emulsion experiment, the projectile singly charged fragment is usually regarded as a proton. In fact, H can be p, d, and t.

Recently, in the EMD of ^{32}S into $\text{H} + \text{P}$ at 200A GeV, a two-temperature structure in the H fragment transverse momentum (P_T) distribution was observed [2]. It is interesting for us to explain this two-temperature structure of the H fragment P_T distribution.

It is generally believed that an EMD corresponds to a collision of two virtual photons with given momenta. The virtual photon energy distributions can be given by the Weizsacker-Williams (WW) method. But the final-state energy (E_f) spectrum measured in the E814 experiment is not well reproduced in both the low and high E_f regions by calculations based on the WW method [7, 8]. Maybe we need another mechanism to explain the E_f spectrum.

In this paper, we introduce a simple model to analyze the experimental H fragment P_T distribution and to give a modelling calculation of the E_f spectrum in the EMD of ${}_Z\text{X}$ into $\text{H} + {}_{Z_i-1}\text{Y}$. The calculated results are compared with the available experimental data [2, 3, 5, 7].

II. The model

II-1. Transverse momentum distribution of relativistic H fragments

In an emulsion experiment, one cannot observe a neutron directly due to the neutrons having no visual track. It is difficult to distinguish p, d and t if we do not have any extra detector. In current emulsion experiments [1-5], $^{32}\text{S}(\circ, \text{n})^{31}\text{S}$ cannot be observed, and $^{32}\text{S}(\circ, \text{p})^{31}\text{P}$ in fact is not distinguished from $^{32}\text{S}(\circ, \text{d})^{30}\text{P}$, $^{32}\text{S}(\circ, \text{pn})^{30}\text{P}$, $^{32}\text{S}(\circ, \text{t})^{29}\text{P}$, $^{32}\text{S}(\circ, \text{dn})^{29}\text{P}$, $^{32}\text{S}(\circ, \text{p2n})^{29}\text{P}$, etc. The different numbers of final nucleons in the above fragmentation channels correspond to different excited energies of the projectile nucleus. It is probable that a multinucleon final state corresponds to a high excited state of the projectile nucleus, and a high temperature emission. That is to say, $^{32}\text{S}(\circ, \text{n})^{31}\text{S}$ and $^{32}\text{S}(\circ, \text{p})^{31}\text{P}$ correspond to a low temperature emission, and the other channels correspond to a relative high temperature emission.

According to our discussion, the temperature of the emission source increases with increasing final state nucleon number, i.e., the excitation energy or virtual photon number. The P_T distribution of the H fragments has more than two temperatures. As a raw estimation, we regard the channel $^{32}\text{S}(\circ, \text{p})^{31}\text{P}$ as the result of low temperature emission, and the channels $^{32}\text{S}(\circ, \text{d})^{30}\text{P}$, $^{32}\text{S}(\circ, \text{pn})^{30}\text{P}$, $^{32}\text{S}(\circ, \text{t})^{29}\text{P}$, $^{32}\text{S}(\circ, \text{dn})^{29}\text{P}$, $^{32}\text{S}(\circ, \text{p2n})^{29}\text{P}$, etc. as the results of high temperature emissions.

Let f denote the emission probability of one proton or neutron. The emission probability of two nucleons is f^2 . The emission probability of three nucleons is f^3 . Considering multinucleon (e.g. m -nucleon) emission, f obeys the following normalization condition,

$$f + f^2 + f^3 + \dots + f^m = 1; \quad (1)$$

The configurations of a one nucleon final state are two: 1p and 1n. The configurations of a two-nucleon final state are three: 2p, 1p1n (p+n, or d) and 2n. The configurations of a three-nucleon final state are four: 3p, 2p1n (p+d, 2p+n, or ^3He), 1p2n (p+2n, d+n, or t), and 3n. For an m -nucleon final state, the configurations are $m + 1$: m p, $(m - 1)p1n, \dots, 1p(m - 1)n$, and m n. In the above configurations, only 1p, 1p1n, 1p2n, $\dots, 1p(m - 1)n$ can be regarded as ${}_Z\text{X}(\circ, \text{H})_{Z_i-1}\text{Y}$ in an emulsion experiment. We have a probability of

$$A = \frac{1}{2}f + \frac{1}{3}f^2 + \frac{1}{4}f^3 + \dots + \frac{1}{m+1}f^m; \quad (2)$$

The probability of low temperature emission H fragments is

$$A_L = \frac{f}{2A}; \quad (3)$$

The probability of high temperature emission H fragments is

$$A_H = 1 - A_L; \quad (4)$$

Our calculation shows that, if we take $m = 3$, then $f \approx 0.54$, $A_L \approx 0.66$, and $A_H \approx 0.34$. If we take $m = 6$, then $f \approx 0.50$, $A_L \approx 0.65$, and $A_H \approx 0.35$. In our calculation, we have found a very interesting equation which will be described in Appendix.

In the rest frame of the emission source, we assume that the three components of particle momentum obey Gaussian distributions having the same standard deviation σ_i . Then the transverse momentum P_T obeys a Rayleigh distribution [6]

$$f_{P_T}(P_T; \sigma_i) = \frac{P_T}{\sigma_i^2} \exp\left(-\frac{P_T^2}{2\sigma_i^2}\right); \quad (5)$$

For a two-source emission process, the P_T distribution is the sum of two Rayleigh distributions

$$f(P_T) = A_L f(P_T; \sigma_{L}) + A_H f(P_T; \sigma_{H}); \quad (6)$$

where σ_L and σ_H are the standard deviations.

II-2. Final-state energy spectrum

We assume that the virtual photons present are isotropically emitted in the electromagnetic field plane of the moving target with high velocity in the rest frame of the projectile. For a given collision parameter, the virtual photon momentum may be different. For a given virtual photon momentum, the final-state products may be different. Generally speaking, if the virtual photon momentum is great, we shall observe a great probability of a multiparticle final-state (a number of protons and neutrons and a few light nuclei emitted from the nucleus). If the virtual photon momentum is small, we shall observe a great probability of single particle final-state (a proton or neutron emitted from the nucleus).

For the process of proton plus residual nucleus, which will be discussed in this paper, we consider that a number of random factors influence the process and assume that the two components of the virtual photon momentum obey Gaussian distributions and have the same width (standard deviation) σ_\circ . Then, the momentum obeys a Rayleigh distribution. For the virtual photon, the energy (E_\circ) equals the momentum due to its zero mass in its rest frame. Therefore, we have the virtual photon energy distribution

$$f_{E_\circ}(E_\circ; \sigma_\circ) = \frac{E_\circ}{\sigma_\circ^2} \exp\left(-\frac{E_\circ^2}{2\sigma_\circ^2}\right); \quad (7)$$

We consider the electromagnetic dissociation process of ^{28}Si into $p + ^{27}\text{Al}$. The final-state energy is the sum of the threshold energy (E_{thr}) for the reaction and the center-of-mass kinetic energies (E_k) of the final-state particles [7], i.e.,

$$E_f = E_k + E_{\text{thr}}; \quad (8)$$

The experimentally reconstructed final-state energy is the excitation energy (E_1^{π}) of ^{28}Si minus the excitation energy (E_R^{π}) of the residual nucleus after the decay, i.e.,

$$E_f = E_1^{\pi} - E_R^{\pi} \quad (9)$$

According to the primary source of the excitation energy, we have the final-state energy

$$E_f = E_0 + Q \quad (10)$$

where $Q = 11.6$ MeV is the combination energy of the last proton in the projectile.

Equations (8-10) are the expressions of the final-state energy. They are different in form due to the different considerations. In Ref. [7], Eq. (9) was used to reconstruct the experimental final-state energy. In this paper, we use Eq. (10) to calculate the theoretical final-state energy. From Eqs. (7) and (10), we have the E_f distribution

$$F(E_f) = \frac{E_f - Q}{\sqrt{\frac{2}{3}}} \exp \left[-\frac{(E_f - Q)^2}{2\frac{2}{3}} \right] \quad (11)$$

III. Comparison with experimental data

Figure 1 presents the transverse momentum distribution for H fragments in the decay mode $^{32}\text{S}(\circ, \text{H})\text{P}$ at 200A GeV. The dotted and solid histograms are the experimental data of Refs. [2] and [3], respectively. The curves are our calculated results. The contributions of low and high temperature emission sources are given by the dashed and dotted curves, respectively. The solid curve is the sum of the dashed and dotted curves. In the calculation, we take $A_L = 0.65$ and $A_H = 0.35$, as described in section 2. The values of $\frac{3}{4}_L$ and $\frac{3}{4}_H$ are obtained by fitting the experimental data and equal 0.16 and 0.47 GeV/c, respectively. The values of $\hat{A}^2/\text{degrees of freedom (DOF)}$ for the above two experimental groups are 0.39 and 0.47, respectively.

Figure 2 presents the transverse momentum distribution for H fragments in the decay mode $^{16}\text{O}(\circ, \text{H})\text{N}$ at 200A GeV. The histograms are the experimental data of Ref. [5]. The curves are our calculated results. The contributions of low and high temperature emission sources are given by the dashed and dotted curves, respectively. The solid curve is the sum of the dashed and dotted curves. In the calculation, we take $A_L = 0.65$ and $A_H = 0.35$ as described in section 2. The values of $\frac{3}{4}_L$ and $\frac{3}{4}_H$ are obtained by fitting the experimental data and equal 0.13 and 0.22 GeV/c, respectively. The value of \hat{A}^2/DOF is 0.55.

From the above comparison we can see that the two-source emission picture gives a good description of the transverse momentum distribution for H fragments in the decay mode ${}_Z\text{X}(\circ, \text{H})_{Z-1}\text{Y}$. The values of $\frac{3}{4}_L$ for different projectile nuclei are nearly the same. But the value of $\frac{3}{4}_H$ increases obviously with increasing projectile nucleus.

For a relative small projectile ^{16}O , the difference between $\frac{3}{4}_L$ and $\frac{3}{4}_H$ is small. The experimental data, in fact, can be described by a single temperature. If we take $\frac{3}{4}_L = \frac{3}{4}_H = 0.15$ GeV/c, the calculated result is shown in Fig. 2 by the dashed-dotted curve. The value of \hat{A}^2/DOF is 1.02. But for a relatively great projectile ^{32}S , the difference between $\frac{3}{4}_L$ and $\frac{3}{4}_H$ is great. The experimental data cannot be described by a single temperature. If we take $\frac{3}{4}_L = \frac{3}{4}_H = 0.17$ GeV/c, the calculated result is shown in Fig. 1 by the dashed-dotted curve. Although the peak position is in agreement with the experimental distribution, the calculated curve cannot reach the tail part of the experimental distribution. The value of \hat{A}^2/DOF is 2827.84.

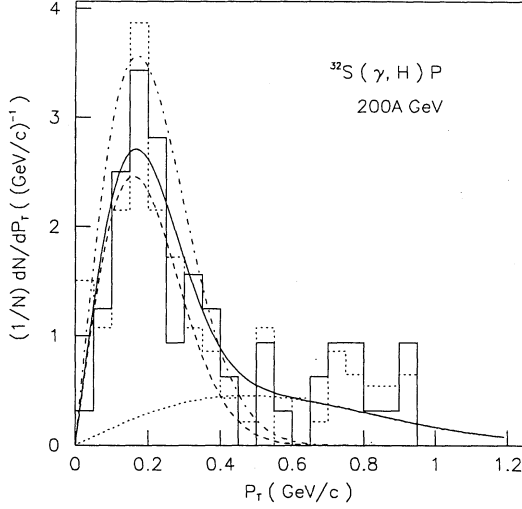


FIG. 1. The transverse momentum distribution for H fragments in the decay mode $^{32}\text{S}(\gamma, \text{H})\text{P}$ at 200A GeV. The dotted and solid histograms are the experimental data of Refs. [2] and [3], respectively. The curves are our calculated results. The dashed and dotted curves are the contributions of low and high temperature emission sources. The solid curve is the sum of the dashed and dotted curves. The dashed-dotted curve shows a single temperature emission.

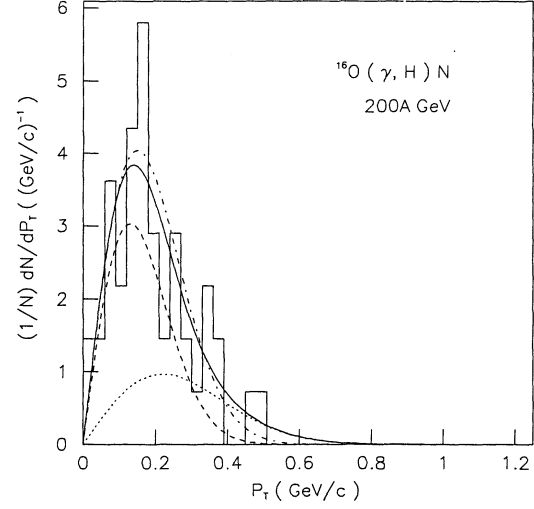


FIG. 2. As for Fig. 1, but showing the result in the decay mode $^{16}\text{O}(\gamma, \text{H})\text{N}$ at 200A GeV. The experimental data are quoted from Ref. [5].

We would like to point out that the fitted curves for the H fragment P_T distributions in the figures of Ref. [2] are not normalized. Obviously, the fitted curves are higher than the experimental histograms. In this case, the value of \hat{A}^2/DOF should be very great. On the other hand, the axis values and labels for the P_T distributions in the figures of Ref. [2] are problematical.

We now compare the calculated final-state energy spectrum with the E814 experimental data on the EMD of ^{28}Si into $p + ^{27}\text{Al}$ at 14.6A GeV. The final-state energy curves obtained from the calculation are shown in Fig. 3 for comparison with the data (histograms with error bars), where the four targets Pb, Sn, Cu, and Al share the same parameter. From fitting the data, we take $\frac{3}{4}\epsilon = 5.2$ MeV. The values of \hat{A}^2/DOF for the above four targets are 0.81, 1.02, 1.54, and 1.39, respectively.

From Fig. 3 one can see that the agreement between the theoretical and experimental curves is very nice, which means that the hypothesis of the model is a good approach to the reality. We also calculated the final-state energy spectra of relativistic ^{28}Si into $n + ^{27}\text{Si}$ and other relativistic nuclei into a $p(n)$ plus residual nucleus, the results obtained from the calculation are in agreement with the experimental data of the E814 collaboration [8].

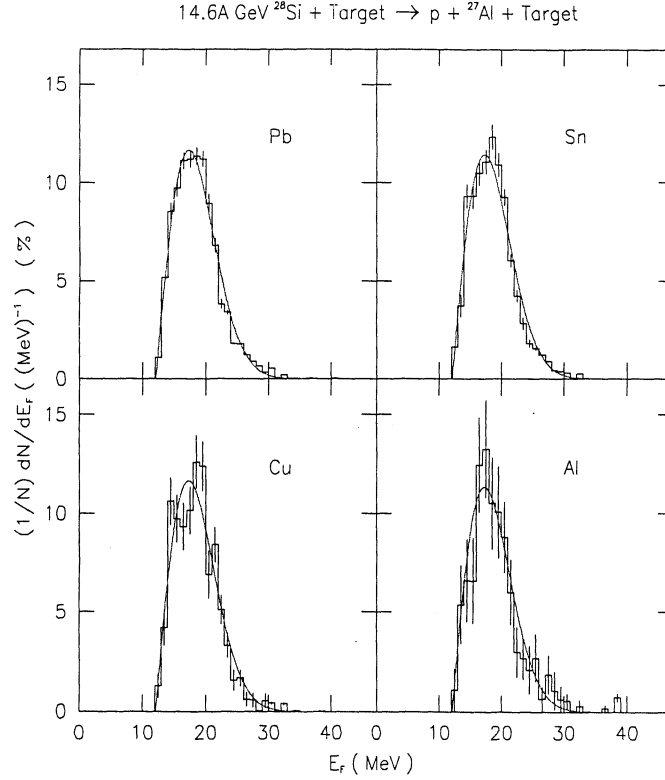


FIG. 3. The final-state energy distributions in the EMD of 14.6A GeV ^{28}Si into p + ^{27}Al for Pb, Sn, Cu, and Al targets. The histograms with error bars are the experimental data of Ref. [7]. The curves are our calculated results.

IV. Conclusions

We have introduced a two-source emission picture to describe the transverse momentum distribution of H fragments in the decay mode ${}^Z\text{X}(\text{H}){}^A\text{Y}$. The calculated results are in agreement with the experimental data of ${}^{32}\text{S}(\text{H})\text{P}$ and ${}^{16}\text{O}(\text{H})\text{N}$ at 200 A GeV. The calculated fractions for low and high temperature emission H fragments are 0.65 and 0.35, respectively. The standard deviations for low and high temperature emission of H fragments in the decay mode ${}^{32}\text{S}(\text{H})\text{P}$ at 200A GeV are 0.16 and 0.47 GeV/c, respectively. The corresponding values for the decay mode ${}^{16}\text{O}(\text{H})\text{N}$ at 200A GeV are 0.13 and 0.22 GeV/c, respectively. The values of $\frac{3}{4}_L$ for different projectile nuclei are nearly the same. But the value of $\frac{3}{4}_H$ increases obviously with increasing projectile nucleus.

For a relative small projectile ${}^{16}\text{O}$, the experimental H fragment P_T distribution, in fact, can be described by a single temperature. But for a relative great projectile ${}^{32}\text{S}$, we have to use the two-source emission picture.

The calculated final-state energy spectrum in the electromagnetic dissociation are in agreement with the experimental data of ${}^{28}\text{Si}$ into p + ${}^{27}\text{Al}$ at 14.6A GeV. The standard deviation of

the final-state energy spectrum is 5.2 MeV. The four targets Pb, Sn, Cu, and Al share the same parameter.

A high energy nucleus-nucleus collision is a very complex process. We need more and better modelling analyses to explain the nuclear reactions and electromagnetic dissociations. The present paper has shown that at relativistic energies it is possible to explain the interaction properties [9, 10] with general physics.

Acknowledgements

The author would like to thank the referee for his comment on Eq. (12) shown in the Appendix and Eq. (2) shown in the section 2.1. This work was supported by the China Scholarship Council, Shanxi Provincial Foundation for Returned Overseas Scholars, Shanxi Provincial Foundation for Leading Specialists in Science, and Shanxi Provincial Science Foundation for Young Specialists.

Appendix: An equation

If a real number x is in the range $[0,1)$, and the integer m is in the range $[2, \max]$, then

$$x^2 = (1 - x) \sum_{m=2}^{\max} x^m; \quad (12)$$

in the large \max limit.

In order to test the above equation, we give the curves of

$$y = x^2 \quad (13)$$

and

$$y = (1 - x) \sum_{m=2}^{\max} x^m \quad (14)$$

in Fig. 4. The dashed curve is Eq. (13) and the dotted curves are Eq. (14) with different \max . For the dotted curves a to b, the values of \max are 5, 10, 20, 50, 100, and 200, respectively.

From Fig. 4 one can see that, if \max is large enough, and x is not too large, Eq. (12) is accurate.

Equation (12) is nothing but the sum of the geometric series. When m is large, the analytical expression for A in Eq. (2) can be easily obtained as

$$A = \frac{1}{f} \ln(1 - f) \quad (15)$$

The asymptotic values are then $\lim_{f \rightarrow 0.5} A = 2 \ln 2 - 1 \approx 0.386$, $\lim_{f \rightarrow 0} A_L = (8 \ln 2 - 4) \approx 1.647$, and $\lim_{f \rightarrow 0} A_H = 1 - \lim_{f \rightarrow 0} A_L \approx 0.353$.

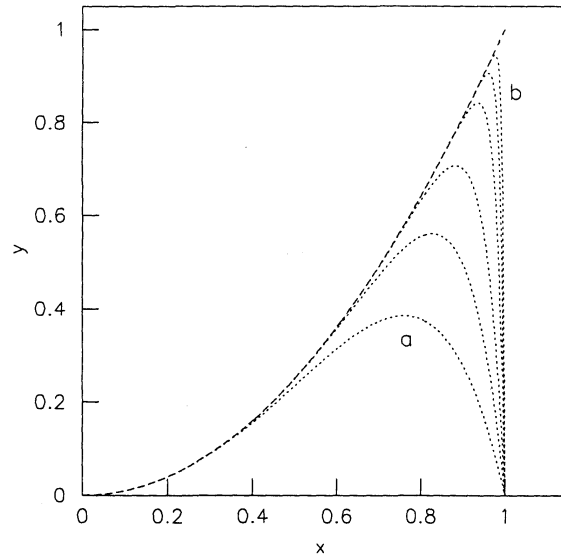


FIG. 4. The curves $y = x^2$ (dashed curve) and $y = (1 - x) \sum_{m=2}^{P_{\max}} x^m$ (dotted curves). From a to b, $\max = 5, 10, 20, 50, 100,$ and $200,$ respectively.

References

E-mail: liufh@dns.sxtu.edu.cn

- [1] F. H. Liu, Ph. D. thesis, China Institute of Atomic Energy, Beijing, China, 1993.
- [2] S. Kamel, Nuovo Cimento A **112**, 327 (1999).
- [3] G. Singh, K. Sengupta and P. L. Jain, Phys. Rev. C **41**, 999 (1990).
- [4] P. Singh, M. Saleem Khan and H. Khushnood, Nuovo Cimento A **111**, 1113 (1998); D. Ghosh *et al.*, Nuovo Cimento A **112**, 277 (1999).
- [5] G. Singh and P. L. Jain, Z. Phys. A **334**, 73 (1992).
- [6] U. A. Abdurazakov *et al.*, Sov. J. Nucl. Phys. **47**, 827 (1988).
- [7] J. Barrette *et al.* (E814 collaboration), Phys. Rev. C **45**, 2427 (1992).
- [8] J. Barrette *et al.* (E814 collaboration), Phys. Rev. C **51**, 865 (1995).
- [9] F. H. Liu, Chin. J. Phys. **38**, 1063 (2000); F. H. Liu, Phys. Rev. C **62**, 024613 (2000).
- [10] F. H. Liu, Chin. J. Phys. **39**, 248 (2001); F. H. Liu, Chin. J. Phys. **39**, 401 (2001).